

**A STUDY OF THE RECORD OF  
ANCIENT SEDIMENTARY ROCKS ON  
MARS USING MER, HIRISE AND CRISM  
IMAGES**

Thesis by

Joannah M. Metz

In Partial Fulfillment of the Requirements for the

degree of

Doctor of Philosophy

CALIFORNIA INSTITUTE OF TECHNOLOGY

Pasadena, California

2010

(Defended March 30, 2010)

© 2010

Joannah M. Metz

All Rights Reserved

## ACKNOWLEDGEMENTS

I am grateful to many people for their support over the last five years at Caltech. First and foremost, I would like to thank my advisor, John Grotzinger, whose encouragement gave me the confidence to turn from a student into a scientist. John has been great at opening doors, and whenever I got stuck he could always put me in touch with the experts or resources that I needed. I also appreciate that John truly cares about his students and has created a very friendly lab environment. I am also thankful for his advice (yes, I did try to read a paper every day), financial support, very helpful comments on all of my papers, and mentoring in the ways of science.

I would like to thank my parents, who have always been willing to listen, even when they had no idea what I was talking about, and to provide an endless source of love and encouragement. I could not have done this without your support.

There are many people at Caltech to whom I am indebted. I would have been lost without the help of Ralph Milliken, who taught me how to work with Mars data, how to use all the software I needed, as well as the principles of spectroscopy. I am also thankful to Ralph for the research discussions and advice. I would like to thank Wes Watters for his patience in teaching me Matlab, as well as Kevin Lewis and Alex Hayes for additional Matlab help. Thanks to Terri Suer for making the DEMs used in this thesis. I would also like to thank Jen Griffes for all of her help in the lab (and for the tasty baked goods). I appreciate the helpful science discussions and feedback from Joann Stock, especially on chapter 5. I would like to thank Oded Aharonson for always taking the time to ask how I was doing, as well as for help to get the DEMs that I needed made. I appreciate Mike Lamb's very helpful comments on chapter 4 as well as his always speedy replies to my questions. I am also grateful to Janice Grancich, Marcia Hudson, and Dian Buchness. You all make Caltech the friendly, caring and supportive environment that it is.

I have been truly fortunate to have undertaken a PhD during a golden age of Mars Exploration when it has first become really possible to apply studies of sedimentary geology to Mars. I have been very lucky to participate in both the Mars Exploration Rover

science team and the HiRISE science team, and I am grateful to Steve Squyres and Alfred McEwen for these opportunities. I would like to thank Gary Kocurek, John Southard, and Steven Fryberger for their helpful comments on chapter 2. I appreciate Douglas Jerolmack and Dave Mohrig's advice on calculating timescales in chapter 3. I would also like to thank Brad Prather, Carlos Pirmez, Alessandro Cantelli, and Ciaran O'Byrne for all of the fantastic discussions about submarine fans and for their suggestions on chapter 4. Thanks to Chris Okubo for the comments on chapter 5.

I cannot imagine making it through these last five years without the support of my friends, both inside and outside of Caltech. Thanks to Dave Fike, Margarita Marinova, Michelle Selvans, Amy Hofmann, and Alejandro Soto for the coffee and lunch breaks that energized me to go back to work, and the interesting discussions to remind me that there's an outside world too. Thanks to the pit crew who helped make our first year fun and not just a lot of hard work. Thank you Woody Fischer for being a great officemate and for all of your advice. Thank you to all of my friends from St. Phillips - you were always there to give me moral support, encouragement, and a home cooked meal. Thanks also to the women of the P.E.O. for your financial and moral support.

## ABSTRACT

Many processes that operate on a planetary surface have the potential to create sedimentary deposits which when preserved as rocks can provide clues that allow past environmental conditions to be reconstructed. This work combines several studies using data from the Mars Exploration Rover and Mars Reconnaissance Orbiter spacecraft to examine the structure and sedimentology of the sedimentary rock record of Mars. The first study supports the dune-interdune model proposed for the formation of the deposits at the *Opportunity* landing site in Meridiani Planum and provides evidence that liquid water was involved to a greater extent in the formation of outcrops in Erebus crater. The next study identifies two depositional fan complexes on the floor of southwestern Melas Chasma and suggests that they may be sublacustrine in origin, which suggests the former presence of a significant body of water stable for at least 100 to 10,000 years. Furthermore, the basin containing the fans may be a complete source-to-sink system. The third study examines the geomorphic channel patterns present on analogue terrestrial submarine fans and deltas. The last study characterizes the extent and styles of deformation of sedimentary rocks in Valles Marineris and finds that subaerial or subaqueous gravitational slumping or sliding and soft-sediment deformation are potential mechanisms that may have caused the deformation.

## TABLE OF CONTENTS

Acknowledgements .....	iii
Abstract .....	v
Table of Contents .....	vi
List of Illustrations .....	ix
List of Tables .....	xii
Acronyms .....	xiii
1 Introduction .....	1
1.1 The Record of Ancient Sedimentary Rocks on Mars .....	1
1.2 Methods .....	4
1.2.1 Datasets .....	4
1.2.1.1 Mars Global Surveyor .....	5
1.2.1.1 Mars Exploration Rovers .....	5
1.2.1.1 Mars Reconnaissance Orbiter .....	7
1.2.2 Software .....	8
1.2.1.1 ArcGIS .....	8
1.2.1.1 ENVI .....	8
1.2.1.1 MATLAB .....	9
2 Sulfate-Rich Bedrock in Erebus Crater, Meridiani Planum .....	12
2.1 Introduction .....	13
2.2 Regional Setting .....	15
2.3 Stratigraphic Framework for Erebus Crater .....	18
2.3.1 Methods .....	18
2.3.2 Results .....	19
2.4 Facies and Depositional Processes .....	24
2.4.1 Mottled Sandstone .....	25
2.4.2 Synsedimentary Deformed Sandstone .....	30
2.4.2.1 Soft-Sediment Deformation .....	30
2.4.2.2 Shrinkage Cracks .....	32
2.4.2.3 Rip-Up Clasts .....	33
2.4.3 Small-Scale Trough Cross-Laminated to Wavy- Laminated Sandstone .....	35
2.4.4 Flat-Laminated to Low-Angle Stratified Sandstone .....	37
2.4.5 Trough Cross-Bedded Sandstone .....	42
2.5 Facies Associations and Depositional Environments .....	43
2.5.1 Eolian Dune .....	43
2.5.2 Eolian Sand Sheet .....	44
2.5.3 Interdune .....	45
2.5.4 Olympia Outcrop Stratigraphy .....	46
2.5.5 Payson Outcrop Stratigraphy .....	47
2.5.6 Yavapai Outcrop Stratigraphy .....	49

2.6 Discussion.....	50
2.6.1 Alternative Interpretations for Depositional Processes.....	50
2.6.1.1 Base Surge.....	50
2.6.1.2 Aqueous Deposition.....	51
2.6.2 Climate Cycles.....	54
2.7 Conclusions.....	58
3 Sublacustrine Depositional Fans in Southwest Melas Chasma.....	60
3.1 Introduction.....	61
3.2 Geologic Setting.....	63
3.3 Methods.....	65
3.4 Descriptions of Fans Used for Comparison.....	67
3.5 Results.....	70
3.5.1 Morphology.....	70
3.5.2 Mineralogy.....	76
3.6 Discussion.....	80
3.6.1 Depositional Fan Comparisons.....	80
3.6.1.1 Alluvial Fans.....	80
3.6.1.2 Gully Deposits.....	81
3.6.1.3 Deltas.....	82
3.6.1.4 Submarine Fans.....	84
3.6.2 Formation of the Melas Western Fans.....	86
3.6.3 Discriminating Between Deltas and Submarine Fans.....	89
3.6.4 Timescales.....	90
3.6.1 Sublacustrine Fans as Terminal Sediment Sinks.....	95
3.7 Conclusions.....	98
4 Geomorphic Channel Patterns on Deltas versus Distal Submarine Fans ...	100
4.1 Introduction.....	101
4.2 Background.....	102
4.3 Study Sites.....	105
4.3.1 Submarine Fans.....	106
4.3.2 Deltas.....	111
4.3.3 Mars fans.....	112
4.4 Data.....	113
4.4.1 Submarine Fans.....	113
4.4.2 Deltas.....	114
4.4.3 Mars Fans.....	114
4.5 Methods.....	115
4.6 Results.....	124
4.7 Discussion.....	127
4.7.1 Nature of Channel Bifurcations.....	127
4.7.2 Mean Channel Length versus Width Trends.....	131
4.7.3 Sinuosity.....	131
4.7.4 Reservoir Model Applications.....	132
4.7.5 Effects of Martian Gravity.....	133
4.8 Conclusions.....	135

5 Thin-Skinned Deformation of Sedimentary Rocks in Valles Marineris.....	136
5.1 Introduction .....	137
5.2 Geologic Setting .....	140
5.3 Methods .....	143
5.4 Results.....	152
5.4.1 Deformation Styles.....	152
5.4.2 Map distribution and stratigraphy of deformed regions.....	157
5.4.2.1 Melas Chasma .....	157
5.4.2.2 Ius Chasma .....	166
5.4.2.3 Candor Chasma .....	167
5.4.3 Elevations of deformed strata .....	169
5.4.4 Fold orientations.....	170
5.4.5 Composition of deformed strata inferred from CRISM spectra	171
5.5 Discussion.....	173
5.5.1 Rheology of deformed strata.....	173
5.5.2 Relative age of deformed strata .....	175
5.5.3 Possible causes of deformation .....	184
5.5.3.1 Liquefaction.....	185
5.5.3.2 Landslides.....	190
5.5.3.3 Regional gravity gliding.....	195
5.6 Conclusions .....	197
References .....	199



## LIST OF ILLUSTRATIONS

<i>Number</i>	<i>Page</i>
1.1 Distribution of layered rocks on Mars .....	3
1.2 Martian timescale .....	4
2.1 Erebus crater location map.....	14
2.2 Payson outcrop facies.....	20
2.3 Yavapai outcrop.....	21
2.4 Geometry of Yavapai beds.....	22
2.5 MI of lower Overgaard.....	23
2.6 Site Topography .....	24
2.7 Stratigraphy of Payson .....	26
2.8 Variation in recrystallization of Payson.....	27
2.9 Prism cracks in lower Overgaard .....	29
2.10 Shrinkage cracks in Bellemont .....	31
2.11 Rip up clasts.....	34
2.12 Wavy and low-angle stratification .....	35
2.13 Stratigraphy of Yavapai .....	38
2.14 Yavapai upper unit .....	40
2.15 Bedform transitions .....	40
2.16 Trough cross-bedding.....	42
2.17 Yavapai lower unit .....	43
2.18 Climate cycles .....	55
3.1 Location map of Southern Melas Basin .....	62
3.2 Melas sublacustrine fans and feature location map.....	71
3.3 Melas fan DEM and dips.....	72
3.4 Melas stratigraphic column .....	73
3.5 Melas fan lobes .....	75
3.6 Melas fan channels .....	76

3.7 Eastern Melas fans.....	77
3.8 CRISM data for Southern Melas Basin .....	79
3.9 Mean channel sinuosity.....	82
3.10 Side-scan sonar image of Mississippi submarine fan.....	84
3.11 Power law fits to length versus width trends .....	88
3.12 Ideal schematic of environments in Southern Melas Basin .....	95
4.1 Location map of fans.....	106
4.2 Channel mapping on side-scan sonar.....	109
4.3 Wax Lake Delta and channel property definitions .....	111
4.4 Mean channel width versus bifurcation order .....	115
4.5 Mean channel length versus bifurcation order .....	116
4.6 Log-log plot of power law fits .....	118
4.7 Plot of channel sinuosity versus bifurcation order .....	124
4.8 Channel branching angle versus bifurcation order .....	125
4.9 Particle settling .....	134
5.1 Location maps .....	142
5.2 Deformation map.....	145
5.3 Deformation styles .....	146
5.4 Histograms of block sizes .....	150
5.5 Valles Marineris stratigraphic columns .....	153
5.6 Basin cross-section .....	156
5.7 Fold axial trace orientations .....	157
5.8 Region 1 southeast map .....	159
5.9 Region 1 southwest map .....	161
5.10 Resistance blocks .....	163
5.11 Gradational contacts .....	165
5.12 Melas slump.....	168
5.13 Light-toned draping deposit in Melas.....	170
5.14 Region 7 east map .....	172
5.15 Region 3 west map .....	173

5.16 Candor DEM .....	175
5.17 CRISM data .....	177
5.18 ILD contacts .....	181
5.19 Landslide volume to runout .....	191

**LIST OF TABLES**

<i>Number</i>	<i>Page</i>
3.1 Characteristics of submarine fans and deltas.....	69
3.2 Characteristics of western Melas fans .....	74
3.3 Depositional fan characteristics .....	83
3.4 Martian alluvial fan gradients .....	99
4.1 Properties of fan systems.....	107
4.2 Channel property measurements.....	118
5.1 Mean block sizes .....	149
5.2 List of CRISM images.....	151
5.3 List of images showing contacts in Valles Marineris.....	183

**ACRONYMS**

**CRISM** Compact Reconnaissance Imaging Spectrometer for Mars

**CTX** Context Camera

**DEM** Digital Elevation Model

**HiRISE** High Resolution Imaging Science Experiment

**MER** Mars Exploration Rover

**MGS** Mars Global Surveyor

**MI** Microscopic Imager

**MOC** Mars Orbiter Camera

**MOLA** Mars Orbiter Laser Altimeter

**MRO** Mars Reconnaissance Orbiter

**THERMIS** Thermal Emission Infrared Spectrometer

## *Chapter 1*

### INTRODUCTION

#### **1.1 The Record of Ancient Sedimentary Rocks on Mars**

Many processes that operate at a planetary surface have the potential to create a record of sedimentary rocks, and these rocks provide clues that allow past environmental conditions to be reconstructed. Earth has a rich sedimentary rock record, and the study of these rocks has provided insights into how the climate of Earth has evolved over the last several billion years. Of all of the planetary bodies in our Solar System, Mars is the only other planet known to have an extensive sedimentary rock record.

While the study of rocks on Mars that appear sedimentary in nature began with Mariner and Viking images (Sharp 1973; Nedell et al. 1987), the field has truly blossomed with the data returned from the Mars Global Surveyor, Mars Odyssey, Mars Express, the Mars Exploration Rovers, and the Mars Reconnaissance Orbiter (Christensen et al. 2000; Malin and Edgett 2000; Malin and Edgett 2003; Glotch et al. 2005; Grotzinger et al. 2005; Ehlmann et al. 2008; Lewis et al. 2008b, Milliken et al. 2008; Metz et al. 2009a; Metz et al. 2009b). With the high-resolution images and spectral data from these spacecraft, the detailed morphology, stratigraphy and composition of sedimentary deposits can now be studied from orbit and on the surface in Meridiani Planum and Gusev crater. Sedimentary rocks from a range of depositional environments have now been identified on Mars, allowing detailed comparisons between environments and processes on Earth and Mars. These environments include eolian dune/interdune (Grotzinger et al. 2005; Metz et al.

2009a), alluvial/fluvial (Mangold et al. 2004; Moore and Howard 2005; Quantin et al. 2005; Kraal et al. 2008a; Mangold et al. 2008a), deltaic (Malin and Edgett 2003; Fassett and Head 2005; Lewis et al. 2006; Wood 2006; Ehlmann et al. 2008; Grant et al. 2008), subaqueous (Metz et al. 2009b) and volcanoclastic (Lewis et al. 2008a).

Many sedimentary environments are quite similar on Earth and Mars; however, there are a few key differences. Because the upper crust of Mars is primarily basaltic instead of intermediate to felsic as on Earth, typical particles derived from chemical weathering on Mars will have a different composition than those on Earth (McLennan and Grotzinger 2008). Chemical and spectral measurements of the rocks exposed on the surface of Mars indicate that many of them were altered in low pH environments dominated by the sulfur cycle, as opposed to moderate pH environments dominated by the carbonate cycle as on Earth (McLennan and Grotzinger 2008). Another key difference between Earth and Mars is that Mars does not have plate tectonics (Albarède and Blichert-Toft 2007; O'Neill et al. 2007), and so sedimentary basins are largely thought to form in impact craters or through rifting, as in Valles Marineris, instead of through subsidence (McLennan and Grotzinger 2008).

Exposures of rocks that may be sedimentary in nature are concentrated in a few areas on Mars, primarily within  $\sim 30^\circ$  of the equator (Fig. 1.1). An ice-rich mantle has been identified on the surface of Mars between  $\sim 30$ - $70^\circ$  north and south and may obscure exposures of sedimentary rocks in those latitude bands (Mustard et al 2001). A survey of High Resolution Imaging Science Experiment (HiRISE) and Mars Orbiter Camera (MOC)

images show that layered rocks occur primarily in Valles Marineris, Meridiani Planum, Arabia Terra, Holden crater and near the western and northern rims of the Hellas impact basin (Malin and Edgett 2000; Griffes et al. 2010). This suggests that at the time these rocks formed, climatic conditions led to stratified rocks primarily deposited in these areas or preferentially preserved or exposed in these areas. Absolute ages for rocks on Mars are

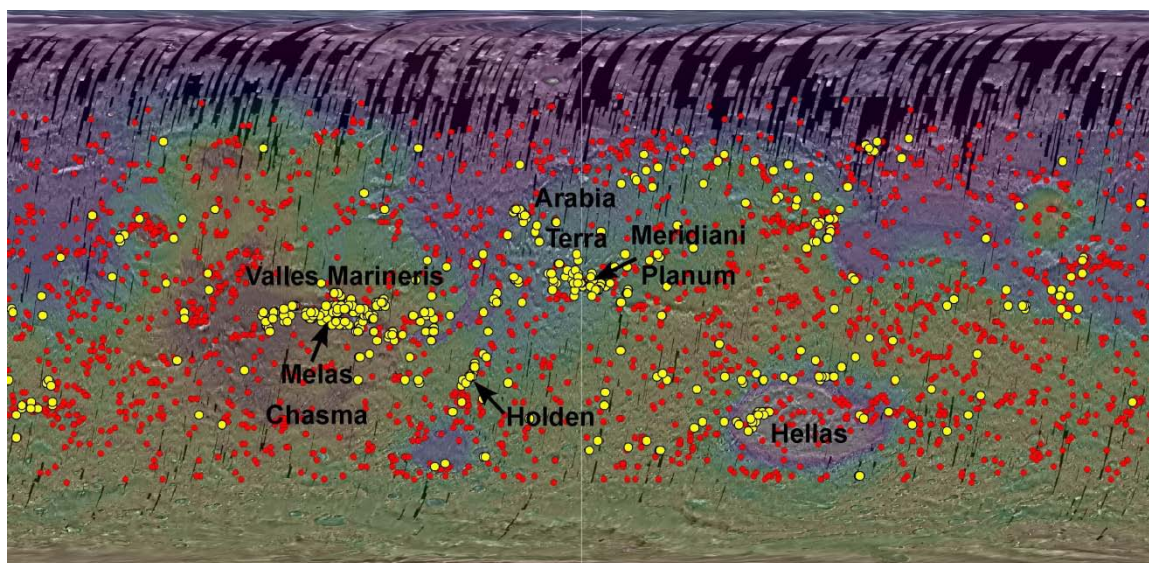


Figure 1.1 MOLA elevation map of Mars overlaid on THEMIS daytime IR mosaic. Red dots indicate locations of HiRISE images that do not show layered deposits. Yellow dots are HiRISE images with stratified bedrock (based on Fig. 1 from Griffes et al. 2010).

not known, but relative ages of rocks can be estimated based on the density of impact craters. Areas that are more heavily cratered are thought to be older and those with fewer impact craters are thought to be younger. Martian time has been divided into three epochs: the Noachian, Hesperian and Amazonian as shown in Figure 1.2.





Figure 1.2 Martian timescale which divides Martian time into three epochs. Noachian refers to rocks older than 3.5 Ga, Hesperian to rocks between 3.5 and 1.8 Ga, and the Amazonian to rocks younger than 1.8 Ga.

The following chapters will describe several exposures of sedimentary rock from different depositional environments on the surface of Mars and will compare them to similar terrestrial environments. Chapter 2 describes eolian dune/interdune facies observed in Erebus crater in Meridiani Planum with the *Opportunity* rover. Chapter 3 describes a depositional fan complex in a small basin in southwestern Melas Chasma, Valles Marineris, and based on similarities to terrestrial depositional fans, infers that it is most likely sublacustrine in origin. Chapter 4 investigates some of the properties of terrestrial submarine fans that serve as a reference for comparison to the Martian sublacustrine fans. Chapter 5 describes many outcrops of deformed sedimentary rocks that are exposed in the central chasmata of Valles Marineris and evaluates potential causes for the deformation.

## 1.2. Methods

The work described in the following chapters uses several datasets and software programs. A short description of the most heavily used datasets is given below along with a description of the software programs.

### 1.2.1 Datasets

### 1.2.1.1 Mars Global Surveyor

The Mars Global Surveyor (MGS) spacecraft was launched in 1996 and operated for nearly a decade before it was lost in November 2006. Data from one of its instruments, the Mars Orbiter Laser Altimeter (MOLA), is used in this thesis, and I refer to data from another of its instruments, the Mars Orbiter Camera (MOC). MOC is a pushbroom camera and includes both a narrow-angle and two wide-angle cameras. Narrow-angle image swaths are roughly 3 km wide and have a ground sampling dimension up to 1.5 m/pixel (Malin et al. 1992). MOLA is an optical remote sensing instrument, and it has acquired the most accurate global topographic map of the surface of Mars to date. MOLA has a vertical accuracy of 1 m and a surface spot size of 168 m with an along track shot spacing of 300 m (Smith et al. 2001).

### 1.2.1.2 Mars Exploration Rovers

The Mars Exploration Rovers (MER) *Spirit* and *Opportunity* landed on the surface of Mars in January 2004, and six years later are still traversing across the surface, long past their nominal 90-sol mission. The *Spirit* rover landed in Gusev crater and the *Opportunity* rover in Meridiani Planum. Each rover contains a suite of scientific instruments including panoramic cameras (Pancam), a microscopic imager (MI), a miniature thermal emission spectrometer (Mini-TES), an alpha particle X-ray spectrometer (APXS), a Mössbauer spectrometer (MB), and a rock abrasion tool (RAT). This thesis primarily uses results from the rover cameras, although key results from the other instruments are summarized.

Pancam is used to provide imaging of the landing sites in order to study the morphology, lithology, texture and distribution of rocks and outcrops. It is a high-resolution color stereo pair of  $1024 \times 1024$ -pixel CCD cameras that are mounted 30 cm apart on a camera bar on top of the rover mast (Bell et al. 2003). The cameras have a  $1^\circ$  toe-in, which means they are angled in, and can provide accurate range data from 5-100 m from the rover (Bell et al. 2003). Each camera has a filter wheel which provides visible and near IR coverage ranging from 400 nm to 1100 nm with stereo imaging available for red (L2/R2) and blue (L7/R1) wavelengths (Bell et al. 2003). The MI is used to provide hand-lens scale imaging of rock and soil textures. It uses the same CCD as the Pancam, but with only a single broad-band filter so images are monochromatic (Squyres et al. 2003). The field of view is  $31 \times 31$  mm with  $30 \mu\text{m}/\text{pixel}$  sampling (Squyres et al. 2003).

The Mini-TES is used to provide mineralogical information for rocks and soils. It is a Michelson interferometer that provides a spectral resolution of  $10 \text{ cm}^{-1}$  over the 5-29  $\mu\text{m}$  range (Squyres et al. 2003). The APXS provides information that can be used to determine the elemental chemistry of rocks and soils, which can be used to help constrain mineralogical analyses. It exposes material to alpha particles and x rays from a radioactive  $^{244}\text{Cm}$  source, and then measures the energy spectra of backscattered alphas and x rays (Squyres et al. 2003). The depth of analysis ranges from 10-100  $\mu\text{m}$ , depending on the atomic number, with a detection limit of 0.5-1 weight percent. The Mössbauer spectrometer can be used to reveal the valence state, molecular structure, and magnetic properties of iron-bearing material in the rocks and soils (Squyres et al. 2003). It uses a  $^{57}\text{Co}$  source and has a depth of sampling of 200-300  $\mu\text{m}$  with a spot size of  $\sim 15$  mm.

The RAT is used to brush dust from rock surfaces and to grind into the surface of rocks to expose fresh material. It is a diamond tipped grinding tool that can remove a cylindrical area of 4.5 cm to a depth of at least 0.5 cm (Squyres et al. 2003).

### 1.2.1.3 Mars Reconnaissance Orbiter

The Mars Reconnaissance Orbiter entered orbit around Mars in 2006 and hosts several high data rate instruments, including the High Resolution Imaging Experiment (HiRISE), the Context Camera (CTX), and the Compact Reconnaissance Imaging Spectrometer for Mars (CRISM). This suite of instruments provides the ability to map the surface of Mars at an unprecedented spatial and spectral resolution. The spacecraft is in a near circular, near polar  $255 \times 320$  km orbit with a mean local solar time of 3:10 pm (Murchie et al. 2007).

The HiRISE camera is a pushbroom camera and has a 6 km swath width and a minimum ground sampling dimension of 25-30 cm/pixel (McEwen et al. 2007). The camera has fourteen  $2048 \times 128$  element CCDs and a 3-color capability over the central 20% of the swath width. MRO has very precise stability and pointing control which allows HiRISE to acquire stereo images that can be combined to form digital elevation models (DEMs) with a vertical precision of ~25 cm (McEwen et al. 2007). The CTX camera acquires context images that can be used for the data acquired by other MRO instruments; it has a 5064 pixel wide CCD array and has a swath width of 30 km with a ground sampling dimension of 6 m/pixel (Malin et al. 2007). The CRISM instrument is a hyperspectral imager that is used to map the mineralogy of key areas of the surface of Mars

at high spatial resolution. In its targeted mode, it has a spatial resolution of 15-19 m/pixel and a spectral resolution of 362-3290 nm at 6.55 nm/channel (Murchie et al. 2007). CRISM uses gimbaling to take out along-track motion of the field of view to allow targeted images of approximately 10 km by 10 km at full spatial resolution (Murchie et al. 2007).

### *1.2.2 Software*

The software programs used most heavily in this thesis (ArcGIS, ENVI, and Matlab) are described below. Additional programs used include Canvas, JMars, and GoogleMars.

#### 1.2.2.1 ArcGIS

Most of the mapping that was done in the following chapters was accomplished in ArcGIS, which is a suite of geographic information system software produced by ESRI. A Thermal Emission Infrared Spectrometer (THEMIS) daytime infrared (IR) global mosaic was used as a basemap and all other images were registered to the basemap using the Mars 2000 projection. HiRISE and CRISM images were manually aligned to CTX images using prominent features in the images.

#### 1.2.2.2 ENVI

CRISM images were processed using the CRISM Analysis Tools (CAT) in ENVI, which is a software application used to process and analyze geospatial imagery. IR and visible images were first converted from PDS format to CAT, then the IR images were

corrected for atmospheric gases and stripes were removed. Band parameter maps were calculated for both IR and visible images, and then the images were projected. Lastly, the IR and visible images were stacked.

CRISM images were analyzed using spectral band parameter maps, which are designed to capture spectral features unique to specific mineralogies (see Table 1 of Pelkey et al. 2007 for a list of CRISM spectral parameters). Band depths generally scale with the abundance of the absorbing mineral, though factors such as particle size and albedo do have an effect (Pelkey et al. 2007). Each band parameter was examined and the three most revealing were combined into the three channels of an RGB image. Regions with interesting features were then selected from a linked RGB band parameter image and the visible image. A spectrally 'neutral' area, often a dusty area, was also selected and the spectra of each region of interest were ratioed to the spectra of the neutral area.

### 1.2.2.3 MATLAB

The DEMs used throughout this thesis were analyzed using scripts I wrote in Matlab; these scripts allow users to directly select bedding planes or contacts in HiRISE DEMs and calculate the orientation of the bedding and the errors on these measurements. The method uses two main steps in order to find the orientation of layers in a DEM. First, a user clicks points along each layer for which the orientation is desired using a graphical user interface. These points are then used to find the orientation of the plane as well as the errors in the measurements.

The inputs to the scripts are a HiRISE orthoimage of the area of interest (along with its worldfile) and a DEM, both in tiff format. Typically, I work with only a subset of the DEM covering a particular portion of interest (usually ~1/3 of the DEM or less) to decrease computing times and memory issues. It is important to select bedding planes or contacts that have three-dimensional exposures so that a unique plane can be fit to the data. It is also important that each bedding plane or contact be relatively planar.

Once the layers have been traced out, the points are used to find a multiple linear regression least-squares plane fit. The equation of the plane is

$$Z = B_1X + B_2Y + B_3 \quad (1)$$

where  $B$  are the coefficients for the multiple linear regression with one-sigma confidence limits,  $X$  is the easting,  $Y$  is the northing and  $Z$  is the elevation. The equation for the strike (in degrees) is

$$dip = \frac{180}{\pi} \tan^{-1} \left( \sqrt{(B_1^2 + B_2^2)} \right), \quad (2)$$

and the equation for the dip (in degrees) is

$$strike = \frac{-180}{\pi} \tan^{-1}(-B_2, B_1) \quad (3)$$

where  $\tan^{-1}$  is the four quadrant inverse tangent. I used bootstrapping with replacement (1000 iterations) to derive the confidence intervals of the strike and dip. This is accomplished by first adding a random residual of the plane fit ( $R^*$ ) to the elevation value, and then subtracting the residual so that the error is not doubled:

$$z^* = z + R^* - R \quad (4)$$

The multiple linear regression is then run using the  $x$ ,  $y$ ,  $z^*$  values, and this is repeated 1000 times. Next, we take the mean of the 1000 strikes and the mean of the 1000 dips derived from the bootstrapping to find the strike and dip, respectively. We then calculate the one-sigma confidence limits on the dip.

Next, we calculate the principal components ( $C_1, C_2, C_3$ ) of the plane fit. I report the colinearity, which is defined as the ratio of the third principal component to the second principal component ( $C_3/C_2$ ). This value should be close to zero for a good plane fit. If the ratio of  $C_3/C_2$  is large, then it means that the points used to define the plane are colinear and the plane should not be used to derive strike and dip measurements.

Two figures are produced from these scripts, (1) shows the image with the location of each selected plane along with a number labeling each plane, and (2) shows the image with the strike and dip symbol and numerical measurement of each plane plotted on top.